

Dual-Color Laser Induced Terahertz Generation in Strong Field Approximation

Kaixuan Zhang,^{1,3} Yizhu Zhang,^{1,2,*} Shuai Li,¹ Xincheng Wang,⁴ Tian-Min Yan,^{1,†} and Y. H. Jiang^{1,3,4,‡}

¹Shanghai Advanced Research Institute, Chinese Academy of Sciences, Shanghai 201210, China

²Center for Terahertz waves and College of Precision Instrument and Optoelectronics Engineering,
Key Laboratory of Opto-electronics Information and Technical Science,

Ministry of Education, Tianjin University, China

³University of Chinese Academy of Sciences, Beijing 100049, China

⁴ShanghaiTech University, Shanghai 201210, China

The mechanism of the terahertz (THz) wave generation (TWG) in dual-color fields is elucidated within the theoretical framework of single-atom based strong field approximation (SFA). Evaluating the transition dipole moment, the continuum-continuum (CC) transition, rather than the continuum-bound recombination for the high-order harmonic generation, is confirmed to be the core mechanism of the TWG. The analytic form of the SFA-based CC description is consistent with the classical photoelectric current model, establishing the quantum-classical correspondence for the TWG. The theory is supported by parametric dependence of experimental THz yields calibrated by the joint measurement of the third-order harmonics. Present studies leave open the possibility of probing the ultrafast dynamics of continuum electron.

Terahertz (THz) wave generation (TWG) using dual-color femtosecond pulse, typically focusing 800 nm and 400 nm beams into gas-phase medium, allows for the convenient and efficient access to moderately strong ultra-broadband THz pulse [1]. Although the approach is widely applied in several disciplines, the underlying generation mechanism is still under discussion [2, 3]. The interpretations so far proposed to unravel the mechanism of TWG, e.g., the four-wave mixing (FWM) and the photocurrent (PC) models, are rather distinctive in their appearances, and the intrinsic physical pictures are completely different. The FWM, as in crystal nonlinear optics [1], explains the nonlinear THz emission based on the quantum perturbation theory, whereas the PC model starting with the plasma formulates the emission process classically [4, 5].

Although the laser plasma is considered the source of the TWG since the first observation from the laser-gas interaction [6], it is still unclear whether the plasma effect is a must ingredient. Similar debate arose in the early days when high-harmonic generation (HHG) was studied. Nowadays it is widely accepted that the HHG is a nonperturbative strong field process dominated by the continuum-bound transition within a single atom or molecule, i.e., recombination of released electron with its parent ion after the ionization. A question naturally arises whether the TWG mechanism can also be clarified by the established strong field theory without the necessity of calling upon plasma effects. If so, the unified theory for both the TWG and the HHG would provide the complementary description of the ionization dynamics, the possible detection scheme and potential applications. In fact, the TWG has been numerically studied by solving time-dependent Schrödinger equation [7–9], ac-

counting for the strong field dynamics of a single atom. Besides, the strong field approximation (SFA), which has been extensively developed to treat various strong field phenomena, including above threshold ionization (ATI), high-order ATI, multiple-ionization, and HHG *et al.*, was also applied to the TWG [10, 11]. However, the link among various theories is still unclear, and the mechanism of the TWG requires more investigation.

In this letter, the origin of the TWG in dual-color fields is inspected by deriving the transition dipole moment under the SFA. The evidences about the dependence of the THz signal on delay-phase and relative polarization angles are presented with the accompanied experiment. The delay dependence between the TWG and third harmonic generation (THG) confirms that the TWG is dominated by the continuum-continuum (CC) transition, rather than the continuum-bound (CB) recombination. Our work has manifold implications. From theoretical aspect, the application scenario of the SFA is further expanded, bringing the TWG explicable under the framework of the strong field physics similar to the HHG. From application aspect, it implies that the TWG is still obtainable through the CC transition even when the neutral atoms are fully depleted by the strong pump laser, showing the possibility to achieve intense THz fields by pumping gas-phase medium with extremely strong laser. Moreover, since the TWG is encoded by the time-dependent information of the continuum electron, it can be used as a spatial-temporal probe in microscopic scale, complementary to HHG spectral lineshape and photoelectron momentum distributions, to trace ultrafast dynamics of continuum electron in atoms and molecules [12].

Quantum mechanically, the radiation is induced by the time variant dipole moment $\mathbf{d}(t) = \langle \Psi(t) | \hat{\mathbf{r}} | \Psi(t) \rangle = \langle \Psi_0 | \hat{U}(t_0, t) \hat{\mathbf{r}} \hat{U}(t, t_0) | \Psi_0 \rangle$ with the time evolution operator \hat{U} and the initial wave function $|\Psi_0\rangle$. Using the Dyson series for \hat{U} , it is shown $\mathbf{d}(t) = \mathbf{d}^{(0)}(t) + \mathbf{d}^{(1)}(t) + \mathbf{d}^{(2)}(t)$

* zhangyz@sari.ac.cn

† yantm@sari.ac.cn

‡ jiangyh@sari.ac.cn

including three components [13]. The first one $\mathbf{d}^{(0)}(t) = -\langle \Psi_0(t) | \hat{\mathbf{r}} | \Psi_0(t) \rangle$ vanishes in the spherically symmetric system. The second term $\mathbf{d}^{(1)}(t) = i \int_{t_i}^t dt' \langle \Psi_0(t) | \hat{\mathbf{r}} \hat{U}(t, t') \hat{W}(t') | \Psi_0(t') \rangle + \text{c.c.}$ describes the transition between CB states. The last term $\mathbf{d}^{(2)}(t) = - \int_{t_i}^t dt'' \int_{t_i}^t dt' \langle \Psi_0(t'') | \hat{W}(t'') \hat{U}(t'', t) \hat{\mathbf{r}} \hat{U}(t, t') \hat{W}(t') | \Psi_0(t') \rangle$ takes the form of CC transition. Since the external light field is intense, the situation enters the scope of the strong field physics and a natural choice to tackle with the problem is the SFA theory. Essentially, the SFA neglects the influence from the Coulomb potential of the ionic core. Hence, \hat{U} can be substituted by $\hat{U}^{(V)}$, the evolution operator of the Volkov state which is the eigenstate of an electron in the external light field alone, to simplify the further derivation. With the SFA, $\mathbf{d}^{(1)}(t)$ is used to describe the HHG, which is essentially the widely used Lewenstein's model of an illustrative interpretation: the atomic ionization is followed by the transition of the continuum electron back to the bound state, more intuitively, the recollision of the released electron to its parent core, yielding the HHG. The contribution of $\mathbf{d}^{(2)}(t)$ to the HHG is usually negligible [13], as only the "hard" recollision leads to photons of high energy, whereas $\mathbf{d}^{(2)}(t)$ is the "soft" transition between continuum states and the energy of the radiation photons is expected to be small. For the THz photons with small energy, the contribution from $\mathbf{d}^{(2)}(t)$ should be considered, though it is rarely mentioned [10, 11]. In this work, the TWG mechanism is investigated based on the analysis of $\mathbf{d}^{(2)}(t)$, which is referred to as the SFA based CC transition (SFA-CC).

With the radiation given by the acceleration form $\ddot{\mathbf{d}}(t)$, we evaluate the emission field from the derived $\mathbf{d}^{(2)}(t)$ (see Supplementary S1 for details),

$$\mathcal{E}(t) \propto \ddot{\mathbf{d}}^{(2)}(t) \equiv \mathbf{a}_1(t) + \mathbf{a}_2(t). \quad (1)$$

The first term

$$\mathbf{a}_1(t) = \mathbf{E}(t) \int_{t_i}^t dt'' \int_{t_i}^t dt' \eta(t', t'') W(t') W^*(t'') e^{iS_{\mathbf{k}', I_p}(t', t'')}, \quad (2)$$

where $\eta(t', t'') = \left(\frac{2\pi}{i(t' - t'')} \right)^{3/2}$ depicts the diffusion of the electronic wave packet, $W(t') = \boldsymbol{\mu}[\mathbf{k}' + \mathbf{A}(t')] \cdot \mathbf{E}(t')$ is the interaction of the electron with the incident light field $\mathbf{E}(t')$. Here $\mathbf{k}' = \mathbf{k}'(t', t'') \equiv -[\boldsymbol{\alpha}(t') - \boldsymbol{\alpha}(t'')]/(t' - t'')$, and $\boldsymbol{\alpha}(t) = \int^t dt' \mathbf{A}(t')$ is the excursion of the electron and $\mathbf{A}(t')$ is the vector potential. The ionization rate is related to $S_{\mathbf{k}', I_p}(t', t'') = \int_{t'}^{t''} dt''' \left\{ \frac{1}{2} (\mathbf{k} + \mathbf{A}(t'''))^2 + I_p \right\}$ with I_p the ionization energy. The presence of both $W(t')$ and $W(t'')$ indicates the two electronic continuum states are involved, and $e^{iS_{\mathbf{k}', I_p}(t', t'')}$ indicates the joint occurrences of these continuum states created by ionization. The second term of Eq. (1) emerges when the emission

time t approaches the ionization time t' ,

$$\mathbf{a}_2(t) = -2\text{Re} \int_{t_i}^t dt' \eta(t, t') W(t) W^*(t') [\mathbf{k}' + \mathbf{A}(t)] e^{iS_{\mathbf{k}', I_p}(t, t')}, \quad (3)$$

which is referred to as the temporal boundary term. Here, $\mathbf{k}' = \mathbf{k}'(t, t')$.

The TWG in dual-color fields is determined by Eqs. (1)-(3). We apply these equations to examine the delay- and polarization-dependence of the TWG, and the results are compared with our experiment. Here, the femtosecond laser with pulse energy of ~ 1.75 mJ and duration of ~ 35 fs passes through a BBO crystal, generating 800/400 nm two-color laser fields with a intensity ratio of 3:1. The two-color laser is then focused by a reflection mirror of 100 mm focal length to ionize the atmospheric air, and the tight focus scheme is adapted so that the propagation effect in plasma is negligible. Throughout the measurement, the 2ω wave is kept s -polarized, while the relative polarization angle θ and time delay τ between the two-color fields can be independently controlled. The vector of the emitted THz electric field, $\mathcal{E}_{\text{THz}}(\tau, \theta)$, is recorded with the electro-optic sampling technique. More experimental details and the definition of observables can be referred from the Supplementary S2. The components of peak-peak (PP) values along the orthogonal polarizations, $S_{\text{THz},s}(\tau, \theta)$ and $S_{\text{THz},p}(\tau, \theta)$ extracted from $\mathcal{E}_{\text{THz}}(\tau, \theta)$, are presented in Fig. 1(a).

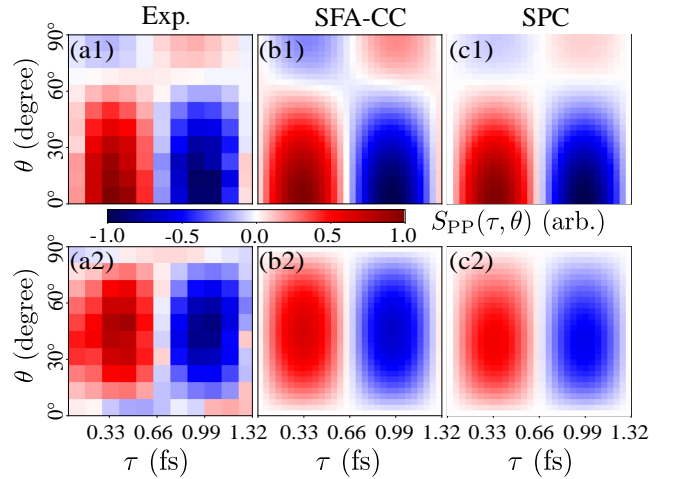


Figure 1. Comparison of PP distributions, $S_{\text{THz},s}(\tau, \theta)$ (upper row) and $S_{\text{THz},p}(\tau, \theta)$ (lower row), respectively, for the s - and p -components of $\mathcal{E}_{\text{THz}}(t)$ obtained from experiment (a) and theoretical models of the SFA-CC (b) and the SPC (c).

Since it is nontrivial to precisely acquire the time delay τ between the two-color fields, a joint measurement of the intensities of the THG, $I_{3\text{rd}}(\tau, \theta)$, is performed. We notice that the THG emissions evaluated with all theoretical models present the similar patterns that the maximum of $I_{3\text{rd}}(\tau, \theta)$ appears at $\tau = 0$ (Supplementary S3). Hence, the time delay zero of the τ -dependent signals can be reliably determined by locating the maximum

of the $I_{3\text{rd}}(\tau, \theta)$.

In our measurement, the τ -dependent distributions $S_{\text{THz},s(p)}(\tau)$ [Fig. 1(a)] and $I_{3\text{rd}}(\tau)$ (Supplementary S3) show the antiphase relationship that the maximum TWG along τ coincides with the minimum THG. On one hand, the distribution in antiphase clearly rules out the contribution from CB transition $\ddot{\mathbf{d}}^{(1)}(t)$, since it contradicts the synchronized distributions of $S_{\text{THz},s(p)}(\tau)$ and $I_{3\text{rd}}(\tau)$ as predicted by $\ddot{\mathbf{d}}^{(1)}(t)$ (see results in Supplementary S4). On the other hand, the PP values from the CC transition $\ddot{\mathbf{d}}^{(2)}(t)$, as shown in Fig. 1(b), well reproduces the salient experimental characteristics, e.g., the decrease and revival of $S_{\text{THz},s}(\tau, \theta)$ when θ increasing, confirming the role of the single atom ionization process in the TWG.

The distribution is also evaluated with the PC model, where the TWG is determined by the time-variant plasma density, $\mathcal{E}_{\text{THz}}(t) \propto \partial j(t)/\partial t = e^2 N(t) \mathbf{E}(t)/m$. The transient electron density $N(t)$ originates from the accumulated electrons from ionization, satisfying

$$\partial_t N(t) = [N_g - N(t)]w(t), \quad (4)$$

where N_g is the initial density of the air, and $w(t)$ is the ionization rate [14]. Thus, $\mathcal{E}_{\text{THz}}(t) \propto N_g \left(1 - \exp\left[-\int^t dt' w(t')\right]\right) \mathbf{E}(t)$ accounts for the residual current induced by the external field in the plasma. The expansion up to the first order of the exponent, i.e.,

$$\mathcal{E}_{\text{THz}}(t) \propto \mathbf{E}(t) \int^t dt' w(t'), \quad (5)$$

however, is essentially based on the single-atomic ionization, since Eq. (5) is the solution of $\partial_t N(t) = N_g w(t)$, where the depletion of the neutral atoms in plasma, $-N(t)w(t)$, as appeared in Eq. (4), is neglected. Therefore, Eq. (5) is referred to as the *single-atom* PC (SPC) model (see Supplementary S5 for comparison of results between PC and SPC). In Fig. 1(c), the distribution from SPC model also shows a good agreement with the experiment in Fig. 1(a).

It is not a coincidence that all these models agree well with the experimental results. As is shown in the followings, there exists a linkage among different theories. Obviously, the SFA-CC and the SPC share the similar form—the rate $w(t')$ in Eq. (5) is simply substituted by $w_1(t'; t)$ in Eq. (2), as defined by $w_1(t'; t) = \int_{t_i}^t dt'' \eta(t', t'') W(t') W^*(t'') e^{iS_{\kappa', I_p}(t', t'')}$. Before showing the correspondence between $w(t)$ and $w_1(t'; t)$, we first examine the distribution of $w_1(t'; t)$ versus the ionization time t' at different emission instants t . As is presented in Fig. 2(a) and inset (c), $w_1(t'; t)$ is nonvanishing only for $t > t'$, as is restricted by the principle of causality that the ionization event should precede the emission. Despite the apparent dependence of $w_1(t'; t)$ on t , the temporal distributions for $t' < t$ remain almost unaltered versus t , except around the boundary when $t = t'$.

Besides $w_1(t'; t)$ for \mathbf{a}_1 , we can also define $w_2(t'; t)$ from \mathbf{a}_2 so that the total contribution of the SFA-

CC, $w(t'; t) = w_1(t'; t) + w_2(t'; t)$, is formally consistent with $w(t)$ in Eq. (5). For the collinear dual-color laser fields, straightforwardly we have $w_2(t'; t) = -2\text{Re}\eta(t, t') W(t) W^*(t') \frac{\kappa' + A(t)}{E(t)} e^{iS_{\kappa', I_p}(t, t')}$. The distribution of $w_2(t'; t)$ is shown in Fig. 2(b) and inset (d). The contribution from $w_2(t'; t)$ is almost negligible, except when $t' \rightarrow t$, that is why it is referred to as the boundary term. It may influence some details of the TWG process, leading to subtle differences between the quantum mechanical SFA-CC and the semiclassical PC models. When t is sufficiently large, the distribution of $w(t'; t)$ is almost equivalent to $w_1(t'; t)$.

With the approximation that the contribution from $w_2(t'; t)$ negligible and $w_1(t'; t)$ roughly independent of t , the $w_1(t'; t)$ versus the ionization time t' can be directly compared with $w(t')$, as shown in Fig. 2(f). Comparing SFA-CC with SPC model, if the emission time t is sufficiently away from t' , $w_1(t'; t)$ versus t' presents the similar distribution as $w(t')$ of the SPC. In other words, $w(t')$ can be considered as the quasi-static limit of the $w_1(t'; t)$ restricted by the time ordering $t' < t$, even though $w(t')$ is introduced from the view of macroscopic photoelectric current, while $w_1(t'; t)$ is derived completely from single-atom based microscopic process of strong field ionization. In explaining the TWG, the SFA and (S)PC theories exhibit the quantum-classical correspondence.

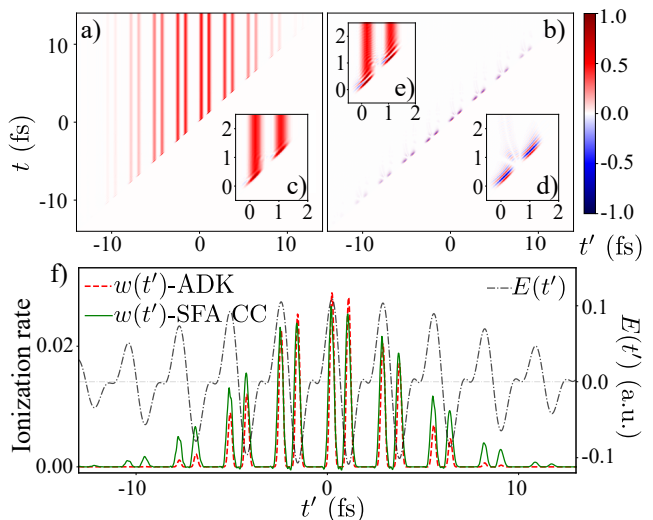


Figure 2. The $w(t'; t)$ of the SFA-CC and the comparison with $w(t')$ of the SPC when $\theta = 0^\circ$ and $\tau = 0.33$ fs. In collinear dual-color laser fields, the SFA-CC derived $w_1(t'; t)$ and $w_2(t'; t)$ are shown in (a) and (b), respectively, with their detailed zoom-in around $t' = 0$ in insets (c) and (d). The total contribution, $w(t'; t) = w_1(t'; t) + w_2(t'; t)$, is presented in inset (e), showing that $w_2(t'; t)$ almost contributes at $t' = t$ only. In (f), $w(t'; t \rightarrow \infty)$ of the SFA-CC (solid line), is compared with $w(t')$ of the SPC (dashed line), showing the correspondence between the SFA based quantum model and the semi-classical PC model.

Besides the formal similarities to the PC model, $\mathbf{a}_1(t)$ in Eq. (2) explicitly shows the third-order dependence

on the external electric field $\mathbf{E}(t)$, as presented by the perturbative third-order response in the FWM model. The response to the incident fields, as predicted in the FWM, can be verified by experimental observations of polarization- and intensity-dependence THz yields [15, 16]. The conventional perturbative FWM susceptibility, however, is replaced by the nonperturbative transition dipole moment induced by strong fields. Thus, the SFA-CC is in concordance with the ionization induced multiwave mixing [9], unifying the existent explanations including FWM the PC models.

In conclusion, the mechanism of the dual-color TWG has been clarified under the theoretical framework of the strong field physics, claiming another success of the renowned SFA theory. Although the ensemble behavior of the laser-induced plasma may influence the radiation yields, the underlying origin of the TWG resides within the scope of nonperturbative single atomic strong field processes. In contrast to the HHG emitted by the CB transition of a recolliding electron, the TWG originates

from the CC transition of a released electron after the ionization. The TWG mechanism of the CC—the "soft" transition—beyond the HHG mechanism of "hard" recollision, is a complement to the radiation theory of the strong field physics. Meanwhile, it is shown that the classical PC model can be derived from the SFA-CC method, bridging between the classical and quantum-mechanical interpretations. Also, the FWM can be reached from the SFA-CC by presenting the explicit third-order dependence on the electric field. Hence, the SFA-CC serves to unify the FWM and PC models, while it offers more microscopic details comparing to the latter coarse-grained models. Our research of the TWG mechanism opens up the possibility to extract the ultrafast dynamics of continuum electron from the ionization-induced THz emission.

The study was supported by National Natural Science Foundation of China (NSFC) (11420101003, 11604347, 11827806, 11874368, 61675213, 91636105). We also acknowledge the support from Shanghai-XFEL beamline project (SBP) and Shanghai High repetition rate XFEL and Extreme light facility (SHINE).

-
- [1] D. J. Cook and R. M. Hochstrasser, *Opt. Lett.* **25**, 1210 (2000).
- [2] V. A. Andreeva, O. G. Kosareva, N. A. Panov, D. E. Shipilo, P. M. Solyankin, M. N. Esaulkov, P. González de Alaiza Martínez, A. P. Shkurinov, V. A. Makarov, L. Bergé, and S. L. Chin, *Phys. Rev. Lett.* **116**, 063902 (2016).
- [3] L.-L. Zhang, W.-M. Wang, T. Wu, R. Zhang, S.-J. Zhang, C.-L. Zhang, Y. Zhang, Z.-M. Sheng, and X.-C. Zhang, *Phys. Rev. Lett.* **119**, 235001 (2017).
- [4] K. Y. Kim, J. H. Glowonia, A. J. Taylor, and G. Rodriguez, *Opt. Express* **15**, 4577 (2007).
- [5] K. Y. Kim, A. J. Taylor, J. H. Glowonia, and G. Rodriguez, *Nat. Photonics* **2**, 605 (2008).
- [6] H. Hamster, A. Sullivan, S. Gordon, W. White, and R. W. Falcone, *Phys. Rev. Lett.* **71**, 2725 (1993).
- [7] N. Karpowicz and X.-C. Zhang, *Phys. Rev. Lett.* **102**, 093001 (2009).
- [8] D. Zhang, Z. Lü, C. Meng, X. Du, Z. Zhou, Z. Zhao, and J. Yuan, *Phys. Rev. Lett.* **109**, 243002 (2012).
- [9] V. A. Kostin, I. D. Laryushin, A. A. Silaev, and N. V. Vvedenskii, *Phys. Rev. Lett.* **117**, 035003 (2016).
- [10] Z. Zhou, D. Zhang, Z. Zhao, and J. Yuan, *Phys. Rev. A* **79**, 063413 (2009).
- [11] T. Balčiūnas, D. Lorenc, M. Ivanov, O. Smirnova, A. M. Zheltikov, D. Dietze, K. Unterrainer, T. Rathje, G. G. Paulus, A. Baltuška, and S. Haessler, *Opt. Express* **23**, 15278 (2015).
- [12] I. Babushkin, A. J. Galan, V. Vaičaitis, A. Husakou, F. Morales, A. Demircan, J. R. C. Andrade, U. Morgner, and M. Ivanov, [arXiv:1803.04187 \[physics\]](https://arxiv.org/abs/1803.04187) (2018), arXiv: 1803.04187.
- [13] W. Becker, A. Lohr, M. Kleber, and M. Lewenstein, *Phys. Rev. A* **56**, 645 (1997).
- [14] M. Ammosov, N. Delone, and V. Krainov, *JETP* **64**, 1191 (1986).
- [15] Y. Zhang, Y. Chen, S. Xu, H. Lian, M. Wang, W. Liu, S. L. Chin, and G. Mu, *Opt. Lett.* **34**, 2841 (2009).
- [16] X. Xie, J. Dai, and X.-C. Zhang, *Phys. Rev. Lett.* **96**, 075005 (2006).

Supplemental Materials: Dual-Color Laser Induced Terahertz Generation in Strong Field Approximation

S1. TRANSITION DIPOLE MOMENT UNDER THE STRONG FIELD APPROXIMATION

The expected value of dipole moment is $\mathbf{d}(t) = -\langle \Psi(t) | \hat{\mathbf{r}} | \Psi(t) \rangle = -\langle \Psi_0(t_i) | \hat{U}(t_i, t) \hat{\mathbf{r}} \hat{U}(t, t_i) | \Psi_0(t_i) \rangle$. With the time evolution operator $\hat{U}(t, t_i)$ expanded by Dyson series, $\hat{U}(t, t_i) = \hat{U}_0(t, t_i) - i \int_{t_i}^t dt' \hat{U}(t, t') \hat{W}(t') \hat{U}_0(t', t_i)$, where $\hat{U}_0(t', t_i)$ is the interaction-free time evolution operator and \hat{W} is the interaction operator, we find that $\mathbf{d}(t) = \mathbf{d}^{(0)}(t) + \mathbf{d}^{(1)}(t) + \mathbf{d}^{(2)}(t)$, where

$$\mathbf{d}^{(0)}(t) = -\langle \Psi_0(t) | \hat{\mathbf{r}} | \Psi_0(t) \rangle, \quad (\text{S1})$$

$$\mathbf{d}^{(1)}(t) = -(-i) \int_{t_i}^t dt' \langle \Psi_0(t) | \hat{\mathbf{r}} \hat{U}(t, t') \hat{W}(t') | \Psi_0(t') \rangle + \text{c.c.}, \quad (\text{S2})$$

$$\mathbf{d}^{(2)}(t) = - \int_{t_i}^t dt'' \int_{t_i}^{t''} dt' \langle \Psi_0(t'') | \hat{W}(t'') \hat{U}(t'', t) \hat{\mathbf{r}} \hat{U}(t, t') \hat{W}(t') | \Psi_0(t') \rangle. \quad (\text{S3})$$

The $\mathbf{d}^{(0)}(t)$ vanishes in a spherically symmetric system. The $\mathbf{d}^{(1)}(t)$, referred to as the continuum-bound (CB) transition dipole moment, depicts the coherent emission at time t induced by the transition of electron from continuum, which accumulates over all possible ionization events at time t' , to the bound state. The $\mathbf{d}^{(1)}(t)$ is widely recognized to dominate the high-order harmonic generation (HHG) process. Similarly, the $\mathbf{d}^{(2)}(t)$, referred to as the continuum-continuum (CC) transition dipole moment, describes the coherent emission induced by the transition between states of continuum, which is often negligible for the HHG calculation. Here, however, we emphasize the role of the $\mathbf{d}^{(2)}(t)$ in terahertz wave generation (TWG). In the followings, the details of $\mathbf{d}^{(1)}(t)$ and $\mathbf{d}^{(2)}(t)$ as used to evaluate the emission are presented.

A. $\mathbf{d}^{(1)}$: Continuum-Bound (CB) Transition

The CB transition $\mathbf{d}^{(1)}(t)$ is given by Eq. (S2). Under the strong field approximation (SFA) which neglects the interaction between the photoelectron and the parent ion, the full time-evolution operator is substituted by the operator with the external light field only, $\hat{U}(t, t') \rightarrow \hat{U}_I(t, t')$, yielding

$$\mathbf{d}^{(1)}(t) = -(-i) \int_{t_i}^t dt' \langle \Psi_0(t) | \hat{\mathbf{r}} \hat{U}_I(t, t') \hat{W}(t') | \Psi_0(t') \rangle + \text{c.c.}$$

with $\hat{U}_I(t, t') = \int d\mathbf{k} |\Psi_{\mathbf{k}}^{(V)}(t)\rangle \langle \Psi_{\mathbf{k}}^{(V)}(t')|$. The Volkov state $|\Psi_{\mathbf{k}}^{(V)}(t)\rangle = |\mathbf{k} + \mathbf{A}(t)\rangle e^{-iS_{\mathbf{k}}(t)}$ with $S_{\mathbf{k}}(t) = \frac{1}{2} \int^t dt' [\mathbf{k} + \mathbf{A}(t')]^2$ and the vector potential $\mathbf{A}(t)$. Considering the interaction $W(t') = \boldsymbol{\mu}[\mathbf{k}' + \mathbf{A}(t')] \cdot \mathbf{E}(t')$ between the electron with the incident electric field $\mathbf{E}(t')$ and substituting $|\Psi_0(t')\rangle = |\psi_0\rangle e^{-iE_0 t'}$, it is shown that $\mathbf{d}^{(1)}(t) = i \int_{t_i}^t dt' \int d\mathbf{k} e^{-iS_{\mathbf{k}, I_p}(t, t')} \boldsymbol{\mu}^*[\mathbf{k} + \mathbf{A}(t)] \mathbf{E}^*(t') \cdot \boldsymbol{\mu}[\mathbf{k} + \mathbf{A}(t')] + \text{c.c.}$, where \mathbf{k} is the intermediate momentum, and $S_{\mathbf{k}, I_p}(t, t') = \int_{t'}^t dt'' (\frac{1}{2} [\mathbf{k} + \mathbf{A}(t'')]^2 + I_p)$ with the ionization energy $I_p = -E_0$. In this work, the 1s state of the hydrogen atom is considered as the initial state for simplicity, the dipole matrix element reads $\boldsymbol{\mu}(\mathbf{k}) = -i2^{\frac{7}{2}} \mathbf{k} / [\pi(k^2 + 1)^3]$, and $I_p = 0.5$ a.u.. The integration over momentum can be approximated with the stationary phase, and the stationary point \mathbf{k}_s is the solution to the equation $\nabla_{\mathbf{k}} S_{\mathbf{k}, I_p}(t, t') \stackrel{!}{=} 0$. Therefore, we obtain the CB transition dipole

$$\mathbf{d}^{(1)}(t) = i \int_{t_i}^t dt' \left(\frac{2\pi}{i(t-t')} \right)^{\frac{3}{2}} \boldsymbol{\mu}^*[\mathbf{k}_s + \mathbf{A}(t)] \mathbf{E}^*(t') \cdot \boldsymbol{\mu}[\mathbf{k}_s + \mathbf{A}(t')] e^{-iS_{\mathbf{k}_s, I_p}(t, t')} + \text{c.c.} \quad (\text{S4})$$

B. $\mathbf{d}^{(2)}$: Continuum-Continuum (CC) Transition

Under the strong field approximation, the substitution $\hat{U}(t, t') \rightarrow \hat{U}_I(t, t')$ yields

$$\mathbf{d}^{(2)}(t) \simeq -(+i)(-i) \int_{t_i}^t dt'' \int_{t_i}^{t''} dt' \langle \Psi_0(t'') | \hat{W}(t'') \hat{U}_I(t'', t) \hat{\mathbf{r}} \hat{U}_I(t, t') \hat{W}(t') | \Psi_0(t') \rangle. \quad (\text{S5})$$

Similar to the manipulation for the CB transition, the expansion arrives

$$\begin{aligned} \mathbf{d}^{(2)}(t) = & -(+i)(-i) \int_{t_i}^t dt'' \int_{t_i}^t dt' \int d\mathbf{k}' \int d\mathbf{k}'' \\ & \times \boldsymbol{\mu}^*[\mathbf{k}'' + \mathbf{A}(t'')] \cdot \mathbf{E}(t'') \langle \mathbf{k}'' + \mathbf{A}(t) | \hat{\mathbf{r}} | \mathbf{k}' + \mathbf{A}(t) \rangle \\ & \times \boldsymbol{\mu}[\mathbf{k}' + \mathbf{A}(t')] \cdot \mathbf{E}(t') e^{-iS_{\mathbf{k}'', I_P}(t'', t)} e^{iS_{\mathbf{k}', I_P}(t', t)}. \end{aligned} \quad (S6)$$

After applying $\langle \mathbf{k}'' + \mathbf{A}(t) | \hat{\mathbf{r}} | \mathbf{k}' + \mathbf{A}(t) \rangle = i\nabla_{\mathbf{k}''} \delta(\mathbf{k}'' - \mathbf{k}')$, the further derivation shows

$$\begin{aligned} \mathbf{d}^{(2)}(t) = & -(+i)(-i)(i)(-1) \int_{t_i}^t dt'' \int_{t_i}^t dt' \int d\mathbf{k}' \boldsymbol{\mu}[\mathbf{k}' + \mathbf{A}(t')] \cdot \mathbf{E}(t') \\ & \times [\nabla_{\mathbf{k}'} - i\nabla_{\mathbf{k}'} S_{\mathbf{k}', I_P}(t'', t)] \{ \boldsymbol{\mu}^*[\mathbf{k}' + \mathbf{A}(t'')] \cdot \mathbf{E}(t'') \} e^{iS_{\mathbf{k}', I_P}(t', t'')}. \end{aligned} \quad (S7)$$

The integration over \mathbf{k}' can also be treated by the stationary phase approximation. Solving the saddle point equation $\nabla_{\mathbf{k}'} S_{\mathbf{k}', I_P}(t', t'') = 0$, we obtain $\mathbf{k}'_s \equiv \mathbf{k}'_s(t', t'') = -[\boldsymbol{\alpha}(t') - \boldsymbol{\alpha}(t'')]/(t' - t'')$ with the excursion $\boldsymbol{\alpha}(t) = \int^t dt' \mathbf{A}(t')$. The approximation with \mathbf{k}'_s results in

$$\begin{aligned} \mathbf{d}^{(2)}(t) = & -(+i)(-i)(i)(-1) \int_{t_i}^t dt'' \int_{t_i}^t dt' \left(\frac{2\pi}{i(t' - t'')} \right)^{3/2} \boldsymbol{\mu}[\mathbf{k}'_s + \mathbf{A}(t')] \cdot \mathbf{E}(t') \\ & \times \{ \nabla_{\mathbf{k}'_s} \boldsymbol{\mu}^*[\mathbf{k}'_s + \mathbf{A}(t'')] - i\boldsymbol{\mu}^*[\mathbf{k}'_s + \mathbf{A}(t'')] \nabla_{\mathbf{k}'_s} S_{\mathbf{k}'_s, I_P}(t'', t) \} \cdot \mathbf{E}(t'') e^{iS_{\mathbf{k}'_s, I_P}(t', t'')}. \end{aligned} \quad (S8)$$

Within the curly bracket, the first term of $\nabla_{\mathbf{k}'_s} \boldsymbol{\mu}^*$ is negligible. Substituting $\nabla_{\mathbf{k}'_s} S_{\mathbf{k}'_s, I_P}(t'', t) = \mathbf{k}'_s(t'' - t) + \boldsymbol{\alpha}(t'') - \boldsymbol{\alpha}(t)$ in the second term,

$$\begin{aligned} \mathbf{d}^{(2)}(t) \simeq & \int_{t_i}^t dt'' \int_{t_i}^t dt' \left(\frac{2\pi}{i(t' - t'')} \right)^{3/2} \\ & \boldsymbol{\mu}[\mathbf{k}'_s + \mathbf{A}(t')] \cdot \mathbf{E}(t') \boldsymbol{\mu}^*[\mathbf{k}'_s + \mathbf{A}(t'')] \cdot \mathbf{E}(t'') \\ & \times \{ \mathbf{k}'_s(t'' - t) + \boldsymbol{\alpha}(t'') - \boldsymbol{\alpha}(t) \} e^{iS_{\mathbf{k}'_s, I_P}(t', t'')}. \end{aligned} \quad (S9)$$

The emission is given by the acceleration $\mathbf{a} = \ddot{\mathbf{d}}^{(2)}(t)$. Applying the Leibniz integral rule, we evaluate the second-order derivative of the dipole moment with respect to t ,

$$\begin{aligned} \ddot{\mathbf{d}}^{(2)}(t) = & \mathbf{E}(t) \int_{t_i}^t dt'' \int_{t_i}^t dt' \left(\frac{2\pi}{i(t' - t'')} \right)^{3/2} e^{iS_{\mathbf{k}'_s(t', t''), I_P}(t', t'')} \\ & \times \boldsymbol{\mu}[\mathbf{k}'_s(t', t'') + \mathbf{A}(t')] \cdot \mathbf{E}(t') \boldsymbol{\mu}^*[\mathbf{k}'_s(t', t'') + \mathbf{A}(t'')] \cdot \mathbf{E}(t'') \\ & - 2\text{Re} \int_{t_i}^t dt' \left(\frac{2\pi}{i(t - t')} \right)^{3/2} e^{iS_{\mathbf{k}'_s(t, t'), I_P}(t, t')} \boldsymbol{\mu}[\mathbf{k}'_s(t, t') + \mathbf{A}(t)] \cdot \mathbf{E}(t) \\ & \times \boldsymbol{\mu}^*[\mathbf{k}'_s(t, t') + \mathbf{A}(t')] \cdot \mathbf{E}(t') [\mathbf{k}'_s(t, t') + \mathbf{A}(t)], \end{aligned} \quad (S10)$$

which is exactly the full form of $\ddot{\mathbf{d}}^{(2)}(t) = \mathbf{a}_1(t) + \mathbf{a}_2(t)$ as presented by Eqs. (2) and (3) in the main text.

S2. EXPERIMENT

The femtosecond amplifier (Libra, Coherent Inc.) delivers a laser pulse with ~ 800 nm center wavelength and ~ 35 fs pulse duration. The pulse with ~ 1.75 mJ is guided into the experiment setup (Fig. S1). The beam with 96% pulse energy is reflected as the pump beam for the terahertz wave generation (TWG), and the transmission beam is used as the probe beam for electro-optic sampling (EOS). The pump beam passes through a 200- μm type-I BBO crystal with the double-frequency efficiency of $\sim 23\%$. The polarization of the laser beam is horizontal (p -polarized), and the optical axis of BBO is kept perpendicular with the laser polarization to obtain the maximum efficiency. The outgoing second harmonic beam is s -polarized. The relative polarization θ between the fundamental ω and second harmonic 2ω beams can be controlled by rotating the zero-order dual-wavelength wave plate (DWP), which acts as a half-wave plate for the ω beam and a full-wave plate for the 2ω beam. The definition of observables is schematically illustrated in Fig. S2. Controlling θ with a half-wave plate, instead of rotating BBO crystal, avoids the mixture of the polarization of ray and ray in the BBO crystal. The ellipticities of both 2ω and ω beams are better than 0.1 when

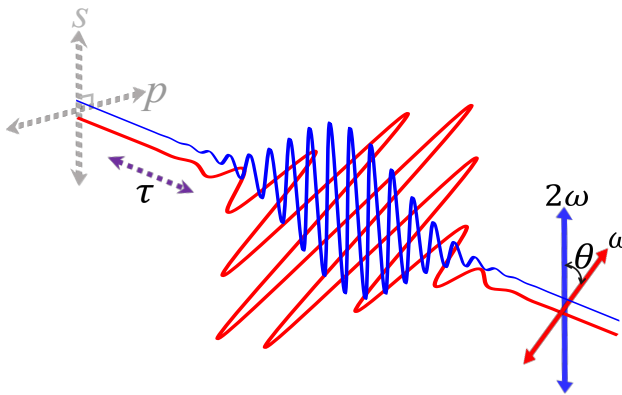


Figure S2. Definition of observables. The 800 nm (ω) and 400 nm (2ω) beams collinearly propagate. The polarization of the 2ω beam is always s -polarized. The relative time delay τ and polarization θ are controlled in the measurement. Both the s - and p -polarized terahertz waves are detected.

S3. DETERMINATION OF TIME DELAY ZERO BY JOINT MEASUREMENT OF THIRD-ORDER HARMONICS

The dependence of TWG on time delay τ between the dual-color fields is critical to determine the TWG mechanisms. For instance, the TWG maximum is predicted to appear at $\tau = 0.33$ fs in the photocurrent (PC) theory, however, at $\tau = 0$ fs in the perturbative four-wave-mixing (FWM) theory. Only when the τ is precisely known, the electric field waveforms for the TWG can be determined for further comparison of the measured data with different theories. However, the precise τ is difficult to obtain, since it is nontrivial to directly monitor the electric fields in practical experiments.

In our experiment, the joint measurement of TWG and THG are conducted. The THG yields along s -polarization $I_{3rd}(\tau, \theta)$ are shown in Fig. S3(a). In addition, we have examined the $I_{3rd}(\tau, \theta)$ evaluated by different theories, including the CB, CC transitions and SPC. All results, as shown in Fig. S3(b)-(d), predict the similar τ dependence that the maximum $I_{3rd}(\tau)$ appears at $\tau = 0$ fs. The time delay zero of dual-color fields in the experiment can therefore be precisely determined by comparison with the theoretical results.

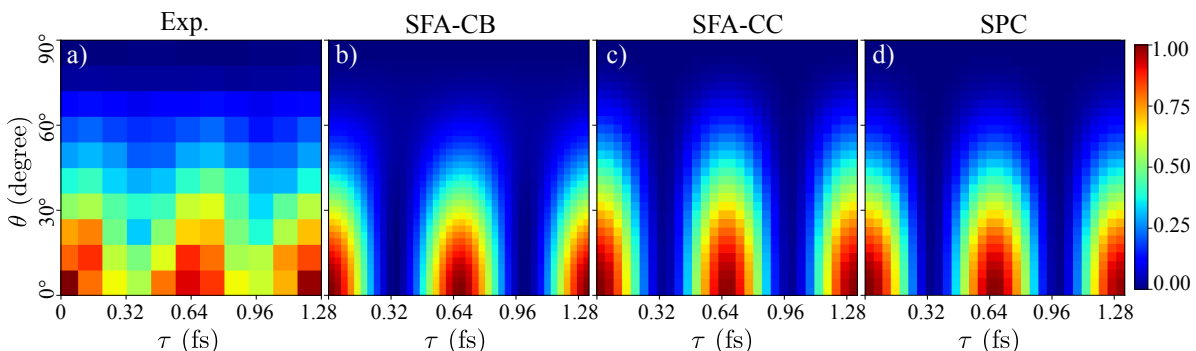


Figure S3. The distribution of the THG along s -polarization $I_{3rd}(\tau, \theta)$ obtained from (a) the measurement, (b) $\ddot{\mathbf{d}}^{(1)}(t)$ of SFA-CB, (c) $\ddot{\mathbf{d}}^{(2)}(t)$ of SFA-CC, and (d) SPC.

S4. CONTINUUM-BOUND TRANSITION IN STRONG FIELD APPROXIMATION

The CB transition is evaluated by Eq. (S4) using the same parameters as in the SFA-CC calculation. For the dual-color laser fields with time delay τ , the electric field $\mathbf{E}(t)$ is given by $\mathbf{E}(t) = \mathbf{E}_\omega(t) + \mathbf{E}_{2\omega}(t - \tau)$. The \sin^2 -envelope is used for the construction of femtosecond pulses. The fundamental field includes 24 cycles with the strength of 0.08 a.u.. The second-harmonic field includes 48 cycles with the strength of 0.046 a.u., assuming BBO has the conversion

efficiency $\sim 30\%$. The $\ddot{\mathbf{d}}^{(1)}(t)$ is Fourier transformed into the frequency domain, and the THz and the third-order harmonic components are filtered out.

The parametric dependence $S_{\text{THz},s(p)}(\tau, \theta)$ predicted by CB transition is shown in Fig. S4.

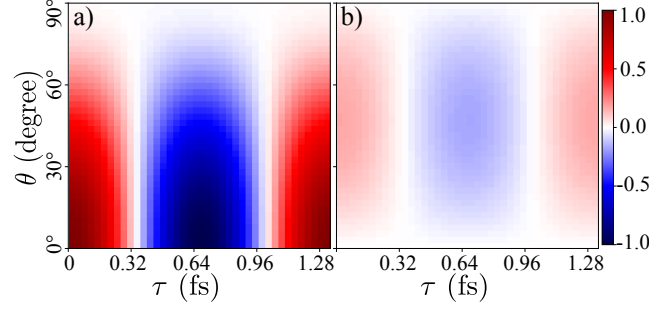


Figure S4. The prediction of CB transition $\mathbf{d}^{(1)}(t)$. (a) and (b) show the s - and p -polarized THz yields $S_{\text{THz},s}^s(\tau, \theta)$ and $S_{\text{THz},s}^p(\tau, \theta)$, respectively.

S5. PHOTOCURRENT AND SINGLE-ATOM PHOTOCURRENT MODEL

In Eq. (5) in the main text, neglecting the neutral depletion is referred to as the single-atom photocurrent (SPC) model. The $S_{\text{THz},s(p)}$ from the SPC model is shown in Fig. 1(c) of the main text. Here, the $S_{\text{THz},s(p)}$ from the traditional PC model is presented in Fig. S5 by comparison. It is shown that there is no significant deviation of the SPC from the PC which involves the neutral depletion.

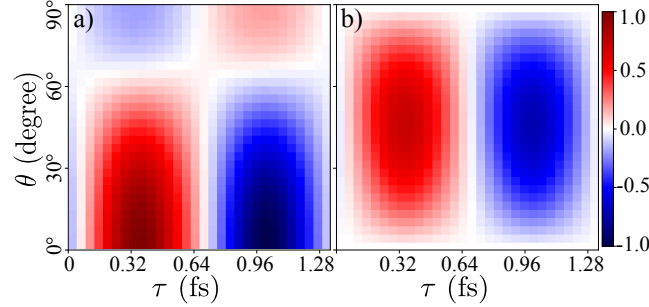


Figure S5. The $S_{\text{THz},s}(\tau, \theta)$ and $S_{\text{THz},p}(\tau, \theta)$ evaluated from the PC model.

For more detailed comparison, slicing the data $S_{\text{THz},s}$ as presented by Figs. (a1), (b1) and (c1) in the main text, the data $S_{\text{THz},s}(\tau = 0.33 \text{ fs}, \theta)$ and $S_{\text{THz},s}(\tau, \theta = 90^\circ)$ from experiment, PC and SPC models are shown in Fig. S6.

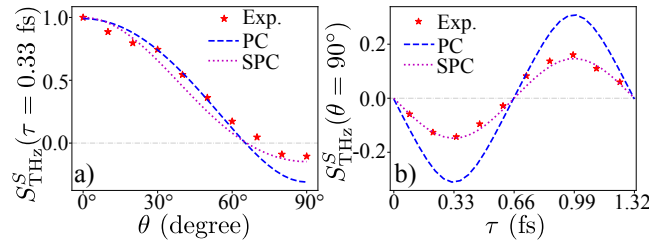


Figure S6. (a) The $S_{\text{THz},s}(\tau = 0.33 \text{ fs}, \theta)$ and (b) $S_{\text{THz},s}(\tau, \theta = 90^\circ)$ of the experiment (red star), PC (blue dashed) and SPC (magenta dotted) models.